Chemical Engineering Journal 150 (2009) 551–554

Contents lists available at ScienceDirect

Chemical Engineering Journal

journal homepage: www.elsevier.com/locate/cej

Preparation and thermal decomposition of $5Mg(OH)_2 \cdot MgSO_4 \cdot 2H_2O$ nanowhiskers

Chuanhui Gao [a,*], Xianguo Li [a], Lijuan Feng [a], Zhanchang Xiang [a], Dahai Zhang [b]

[a] Key Laboratory of Marine Chemistry Theory and Technology, Ministry of Education, Ocean University of China, Qingdao 266100, China
[b] Department of Chemistry, School of Science, The University of Tokyo, 7-3-1 Hongo, Bunkyo, Tokyo 113-0033, Japan

ARTICLE INFO

Article history:
Received 17 September 2008
Received in revised form 7 December 2008
Accepted 19 December 2008

Keywords:
Magnesium hydroxide sulfate hydrate (MHSH) nanowhisker
Hydrothermal synthesis
Thermal decomposition mechanism and kinetics

ABSTRACT

Magnesium hydroxide sulfate hydrate (MHSH) nanowhiskers were prepared using magnesium chloride, ammonia and magnesium sulfate as raw materials by hydrothermal synthesis without any additional template. X-ray powder diffraction (XRD), transmission electron microscopy (TEM) and thermal analysis (TG-DTA) were employed to characterize the composition and structural features of the MHSH nanowhiskers. It is shown that the thermal decomposition of nanowhiskers followed a three-step scheme. Based on DTA data, the reaction order, activation energy and pre-exponential factor for each step were calculated using a non-isothermal Kissinger method. It is also indicated from Satava method that the first step of the thermal decomposition of nanowhiskers is an A_2 nucleus formation and growth mechanism with integral form of $G(a) = [-\ln(1-a)]^{1/2}$. The second step is an A_u branching nuclei mechanism with integral form of $G(a) = \ln[a/(1-a)]$, and the final step is a $P_{1/2}$ nucleation mechanism with integral form of $G(a) = a^{1/2}$.

1. Introduction

MHSH whiskers, first discovered in nature in a submarine geothermal system in 1978, have attracted much attention because of their potential application as resin additives of flame retardant, fillers, or reinforcers [1,2]. MHSH can also be called basic magnesium sulfate or a solid solution in the $xMg(OH)_2 \cdot yMgSO_4 \cdot zH_2O$ system. By varying the ratio of these three constituents, the family of MHSH comprises no less than 20 members. Most works on MHSH compounds in the literature were concentrated on their preparation and characterization [3–9]; although some involve the three decomposition steps of the whisker, there are no further studies on the mechanism and kinetics of the thermal decomposition of MHSH. In this paper, the decomposition mechanism and kinetic parameters of the whisker were studied for the first time. Flame retardant is one of the most important applications of MHSH, further study of this paper on the decomposition process would provide useful data for the research of the flame retardant mechanism and evaluation of the flame retardant effect.

The MHSH nanowhiskers were prepared by hydrothermal method, and the sample was determined as $5Mg(OH)_2 \cdot MgSO_4 \cdot 2H_2O$ [10]. XRD, TEM and TG-DTA were employed to characterize the composition and structural features of the MHSH nanowhiskers. In order to further study the thermal decomposition of MHSH whiskers, Satava method [11,12] was used to study the thermal decomposition mechanism of the whiskers, and the values of kinetic parameters, i.e., the reaction order, activation energy and pre-exponential factor for each of the three steps were evaluated using the Kissinger method [15–18].

2. Experimental

2.1. Preparation of MHSH nanowhiskers

The MHSH nanowhiskers were synthesized by hydrothermal method in autoclave without additional template. 100 mL of ammonia solution ($4.0\ mol\ L^{-1}$) was added dropwise into 200 mL magnesium chloride ($2.0\ mol\ L^{-1}$) at room temperature. The slurry was filtered and the solid was transferred to the autoclave, then 100 mL of magnesium sulfate ($0.5\ mol\ L^{-1}$) was added to the autoclave and kept stirred (400 rpm). The autoclave was heated gradually to 170 °C and maintained the temperature for 3 h. A white precipitate was obtained after the autoclave was cooled down to the room temperature. After filtration, the precipitate was washed with distilled water for several times and then dried in a vacuum oven at 100 °C for 3 h to obtain the product.

2.2. Chemical analysis

In order to determine the composition of the prepared sample, the MHSH sample was dissolved in a given excess standard

* Corresponding author at: College of Chemistry and Chemical Engineering, Ocean University of China, Songling Road, 238, Qingdao, China. Tel.: +86 532 66782215; fax: +86 532 66782540.
E-mail addresses: chuanhuigao@126.com, chuanhuigao@live.cn (C. Gao).

1385-8947/$ – see front matter © 2009 Elsevier B.V. All rights reserved.
doi:10.1016/j.cej.2008.12.029

Table 1
Chemical composition of MHSH.

Mass fraction/ω %	Calculated composition for theoretical MHSH whiskers		Experimental results
	5-1-3	5-1-2	
Mg^{2+}	30.30	32.56	32.03
SO_4^{2-}	20.69	21.52	20.67

HCl solution which was prepared with azeotropic hydrochloric acid and deionized water, and its concentration was determined by titration with standard borax. Magnesium was titrated by a standard solution of Na–EDTA in an alkaline pH 10 buffer solution (ammonium hydroxide + ammonium chloride). SO_4^{2-} was determined by the $BaSO_4$ gravimetric method. From the results of Table 1, we can see that the typical chemical analysis results of the MHSH sample were in agreement with the theoretical values of 5-1-2MHSH, and correspond to a molar ratio $Mg(OH)_2$:$MgSO_4$ = 5:1.

2.3. Characterization

X-ray powder diffraction (XRD) pattern was obtained with a Rigaku D/max-rA X-ray diffractometer with graphite monochromatized Cu K_α radiation. Phase identification of the product during the thermal decomposition of MHSH nanowhiskers was carried out using the XRD pattern shown in Fig. 1. In Fig. 1a, all diffraction peaks can be indexed with respect to the orthorhombic structure $5Mg(OH)_2 \cdot MgSO_4 \cdot 2H_2O$. The structure of the product heated at temperatures about 500 °C could be $5MgO \cdot MgSO_4$ and the diffraction peaks of the final product heated at temperatures

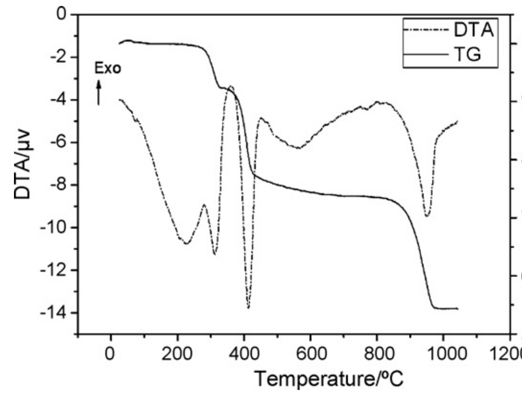

Fig. 3. The TG-DTA curve of $MgSO_4 \cdot 5\,Mg(OH)_2 \cdot 2H_2O$.

higher than 1000 °C were consistent with the XRD pattern of MgO.

Structure and morphology of the product during the thermal decomposition process were observed by TEM. A typical TEM image of the sample is illustrated in Fig. 2. The MHSH nanowhiskers display rod-like morphology with a diameter of 10–100 nm and an aspect ratio between 50 and 200. At temperatures about 500 °C, the products were fibres shorter than 400 nm. At temperatures about 1000 °C, the products were porous crystallized magnesium oxide whiskers.

Thermo-gravimetric analyzer (TGA, ZRY-2P, Shanghai Precision Scientific Instrument Co., Ltd., PR China) was used to characterize the thermal behavior of the nanowhisker products.

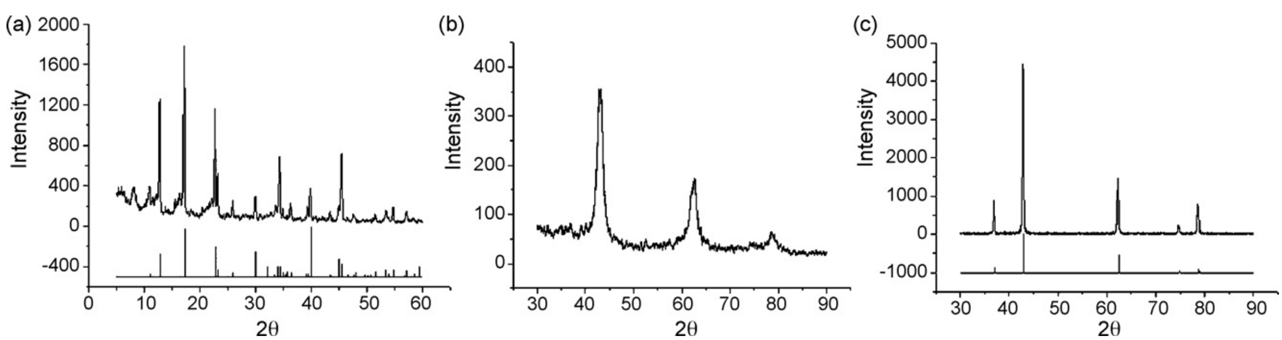

Fig. 1. Typical XRD pattern of the synthesized MHSH nanowhiskers (a), heated at 500 °C (b) and heated at 1050 °C (c). The Bottom curves in (a) and (c) are the standard diffraction patterns of the main diffraction peaks of $5Mg(OH)_2 \cdot MgSO_4 \cdot 2H_2O$ and MgO as reference respectively.

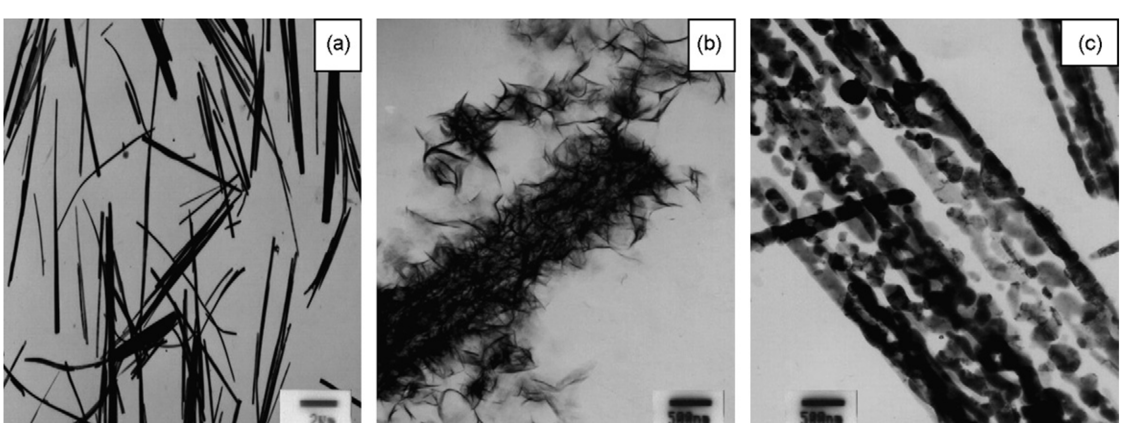

Fig. 2. TEM images of the synthesized MHSH nanowhiskers (a), heated at 500 °C (b) and heated at 1050 °C (c).

Table 2
Calculated mass loss and observed mass loss in TGA thermogram for different steps.

Step	Temperature range/°C	Peak temperature/°C	Calculated mass loss/%	Observed mass loss/%
I	283–392	390	8.07	7.86
II	404–505	459	20.18	19.74
III	910–1081	1049	17.94	17.63

3. Results and discussion

As can be seen from Fig. 3, there were three distinct steps in the overall thermal decomposition process of MHSH nanowhiskers. Two crystal water moieties were lost at the first step. Dehydration resulting in the formation of $5MgO{\cdot}MgSO_4$ occurred at the second step by losing five hydroxyl water molecules from the hydroxyl group. At the last step, MgO whiskers were formed by releasing sulfur trioxide. The experimental weight loss of the three steps were 7.86%, 19.74%, 17.63% which were in agreement with theoretical values 8.07%, 20.18%, 17.94% respectively. The decomposition scheme was shown below, and the observed weight losses shown in Table 2 corresponded very well with these hypothesized steps.

Step I

$$5Mg(OH)_2{\cdot}MgSO_4{\cdot}2H_2O \rightarrow 5Mg(OH)_2{\cdot}MgSO_4 + 2H_2O$$

Step II

$$Mg(OH)_2{\cdot}MgSO_4 \rightarrow 5MgO{\cdot}MgSO_4 + 5H_2O$$

Step III

$$5MgO{\cdot}MgSO_4 \rightarrow 6MgO + SO_3$$

3.1. Determination of the decomposition mechanism

Satava [11,12] method was used to determine the mechanism of the thermal decomposition reaction. Briefly, it is assumed that a function of conversion, $G(a)$, exists for each step of the thermal decomposition reaction. If $G(a)$ could correctly describe the thermal decomposition mechanism of a solid, a plot of $G(a)$ against $1/T$ should give a straight line. According to this method, several algebraic expressions of the most common reaction mechanisms in solid-state reactions [13,14] presented in Table 2 were cited to determine the most probable mechanism of the decomposition process Table 3.

The original mass loss versus temperature curves obtained at constant heating rate were transformed into the degree of conversion (a) versus temperature curves by using the following equation $a=(m_i-m_\tau)/(m_i-m_f)$, where m_i, m_f and m_τ represent the initial, final and current mass of the solid sample at time τ (or temperature T), respectively. The correlation coefficients were obtained from plots of different expressions of $G(a)$ versus $1/T$. The best correlation coefficient of linear regression R^2 was used to estimate the most probable mechanism.

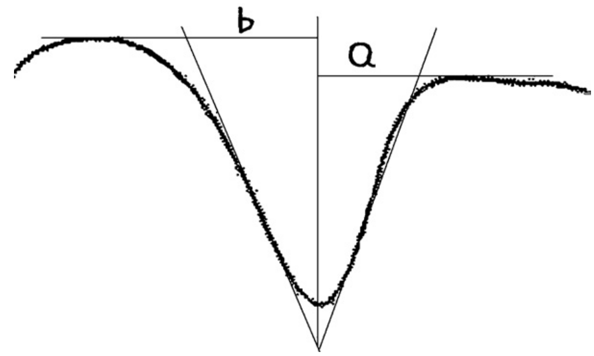

Fig. 4. Sketch diagram for obtaining the peak shape index *I*.

For the first step, the correlation coefficient of function A_2 was the highest. It is therefore speculated that nucleus formation and growth of Avrami–Erofeev function ($n=2$) with integral form of $G(a)=[-\ln(1-a)]^{1/2}$ could be the most probable mechanism. For the second step, the highest correlation coefficient was obtained for function A_u with integral form of $G(a)=\ln[a/(1-a)]$, which corresponds to a branching nuclei mechanism. The third step was characterized by function $P_{1/2}$ with integral form of $G(a)=a^{1/2}$ and its mechanism is nucleation.

3.2. Decomposition kinetics of MHSH

Kinetic parameters for the thermal decomposition of MHSH nanowhiskers were determined by using Kissinger method [15–18]. The three formulas listed below were basic principles:

the mass action law:

$$\frac{da}{dt} = k(1-\alpha)^n \tag{1}$$

the Arrhenius formula:

$$k = \frac{A}{\beta}\exp\left(-\frac{E}{RT}\right) \tag{2}$$

the heating rate formula:

$$\beta = \frac{dT}{dt} \tag{3}$$

In the three formulas, a is the decomposition extent, t is decomposition time, n is reaction order, k is the rate constant, E is the activation energy, A is the pre-exponential factor and R is the gas constant.

Table 3
Algebraic expressions of $G(a)$ and the correlation coefficients for the three decomposition steps.

Symbol	Function name	Mechanism	$G(a)$	Correlation coefficient R^2		
				I	II	III
$F_{1/3}$	One-third order	Chemical reaction	$1-(1-a)^{2/3}$	0.9670	0.9137	0.9241
$P_{1/2}$	Mainpel power law	Nucleation	$a^{1/2}$	0.8927	0.9681	0.9964
$P_{1/3}$	Mampel power law	Nucleation	$a^{1/3}$	0.8577	0.9684	0.9882
A_1, F_1	Avrami–Erofeev equation	Random nucleation and its subsequent growth, $n=1$	$-\ln(1-a)$	0.9407	0.8097	0.6699
A_2	Avrami–Erofeev equation	Random nucleation and its subsequent growth, $n=2$	$[-\ln(1-a)]^{1/2}$	0.9931	0.9366	0.8686
D_1	Parabola law	One-dimensional diffusion	a^2	0.9430	0.8491	0.8541
A_u	Prout–Tomkins equation	Branching nuclei	$\ln[a/(1-a)]$	0.9770	0.9917	0.9035

Table 4
Kinetic parameters from Kissinger method for thermal decomposition of MHSH nanowhiskers.

Heating rate/°C min^{-1}	Step I				Step II				Step III			
	5	10	15	20	5	10	15	20	5	10	15	20
a/mm	3.2	3.2	7.0	8.0	3.0	3.6	4.2	5.0	1.2	1.6	5.5	5.0
b/mm	7.4	3.8	5.8	5.0	14.6	14.6	10.5	10.0	6.5	7.1	15.0	17.0
I	0.432	0.842	1.207	1.600	0.205	0.247	0.400	0.500	0.185	0.216	0.367	0.294
n	0.828	1.155	1.385	1.594	0.571	0.626	0.796	0.891	0.542	0.586	0.764	0.683
Average of n	1.2				0.7				0.6			
E/kJ mol^{-1}	277.6				492.3				797.6			
A	1.926×10^{13}				1.050×10^{26}				1.954×10^{23}			

In terms of the Kissinger principle, assuming that the reaction velocity is maximum at peak temperature,

$$\frac{d(da/dt)}{dt} = 0 \tag{4}$$

so for $T = T_{max}$ (where T_{max} is the maximum temperature of the peak), according to mass action law (1), the Arrhenius formula (2) and heating rate formula (3), formula (5) can be deducted.

$$\frac{E}{RT_{max}^2} = \frac{An}{\beta}(1 - a_{max})^{n-1} \exp\left(-\frac{E}{RT_{max}}\right) \tag{5}$$

Kissinger believes: $n(1 - a_{max})^{n-1}$ has nothing to do with β, and its approximate value is 1, then formula (5) can be rewritten as

$$\ln\left(\frac{\beta}{T_{max}{}^2}\right) = \ln\left(\frac{RA}{E}\right) - \frac{E}{R}\frac{1}{T_{max}} \tag{6}$$

For a certain reaction, the frequency factor A is constant, and $\ln(RA/E)$ is also a constant. The plot of $\ln(\beta/T_{max}{}^2) \sim (1/T_{max})$ is a line and the slope is $(-ER^{-1})$, the intercept $\ln(RA/E)$.

In terms of the Kissinger principle, the shape index I is defined as the absolute value of the ratio of the slops of tangents to the curve at the inflexion points.

$$I = \frac{a}{b} \tag{7}$$

(a and b are lined out in Fig. 4).

The relationship between I and n is

$$I = 0.63n^2 \tag{8}$$

Then the reaction order n can be calculated using formula (8).

For each DTA curve (shown in Fig. 3), a vertical line at each peak was drawn. Values of a and b were then determined as shown in Fig. 4, and the peak shape index I can be calculated with $I = a/b$. The reaction order n was obtained by applying equation $I = 0.63n^2$. The average of n at different heating rates was taken for each step and the results were shown in Table 4.

DTA peak temperatures change with different heating rates(β). According to Kissinger method [15–18], the activation energy E and pre-exponential factor A were obtained from a plot of $\ln(\beta/T_{max}{}^2)$ against $1/T_{max}$. Values of E and A for the three steps of thermal decomposition of MHSH nanowhiskers were shown in Table 4.

As can be seen from Table 4 that from the view of chemistry reaction dynamics, because the activation energy of the first decomposition step was smaller than 300 kJ mol^{-1}, the precursor can become the intermediate $5Mg(OH)_2{\cdot}MgSO4$ in a short time, i.e., the crystal water moieties can be easily lost. The activation energy of the second and third decomposition steps were 492.3 and 797.6 kJ mol^{-1} larger than that of the first step. So the first step of the thermal decomposition of $5Mg(OH)_2{\cdot}MgSO_4{\cdot}2H_2O$ may be interpreted as a “fast” step while the second and third steps as “slow” steps.

4. Conclusions

MHSH nanowhiskers with a diameter of 10–100 nm and an aspect ratio between 50 and 200 were synthesized by hydrothermal method. The thermal decomposition process of MHSH nanowhiskers consists of three distinct steps. By applying Satava method, it is speculated that the most probable mechanisms for the three steps are A_2 nucleus formation and growth, A_u branching nuclei and $P_{1/2}$ nucleation, respectively. The reaction orders, activation energies and pre-exponential factors are 1.2, 277.6 kJ mol^{-1} and 1.926×10^{13} for the first step; 0.7, 492.3 kJ mol^{-1} and 1.050×10^{26} for the second step; and 0.6, 797.6 kJ mol^{-1} and 1.954×10^{23} for the final step.

Acknowledgement

Authors wish to acknowledge Science and Technology Bureau of Qingdao for financial support to this work under project No. 06-2-2-14-jch.

References

[1] J.L. Bischoff, W.E. Seyfried, Am. J. Sci. 60 (1999) 17102.
[2] D.R. Janecky, W.E. Seyfried Jr., Am. J. Sci. (1983) 283.
[3] T. Yue, S.Y. Gao, L.X. Zhu, et al., J. Mol. Struct. 616 (2002) 247.
[4] Y. Ding, H.Z. Zhao, Y.G. Sun, et al., J. Inorg. Mater. 3 (2001) 151.
[5] Y. Ding, G.T. Zhang, S.Y. Zhang, et al., Chem. Mater. 12 (2000) 2845.
[6] X.X. Yan, D.L. Xu, D.F. Xue, Acta Mater. 55 (2007) 5747.
[7] L. Xiang, F. Liu, J. Li, et al., Mater. Chem. Phys. 87 (2004) 424.
[8] Z.Q. Wei, H. Qi, P. Ma, et al., Inorg. Chem. Commun. 5 (2002) 147.
[9] L.X. Zhu, T. Yue, S.Y. Gao, et al., Chin. J. Inorg. Chem. 19 (2003) 99.
[10] L.J. Feng, D.H. Zhang, X.G. Li. Method of Producing Fibrous Magnesium oxide. CN 1766178A.
[11] R.Z. Hu, Q.Z. Shi, Thermal Analysis Kinetics, Beijing, 2001.
[12] Y. Satava, J.J. Sestak, Therm. Anal. 8 (1975) 477.
[13] L. Liqing, C. Donghua, J. Therm. Anal. Cal. 78 (2004) 283.
[14] J.J. Zhang, L.G. Ge, X.L. Zha, Y.J. Dai, H.L. Chen, L.P. Mo, J. Therm. Anal. Cal. 58 (1999) 269.
[15] Z.Q. Cai, Thermal Analysis, Beijing, 1993.
[16] H.E. Kissinger, J. Res. Nat. Bur. Stand. 57 (1959) 712.
[17] H.E. Kissinger, Anal. Chem. 29 (1957) 1702.
[18] L.H. Yue, D.L. Jin, D.Y. Lu, et al., Acta Phys. 7 (2005) 752.